This is an open access article published under an ACS AuthorChoice License, which permits copying and redistribution of the article or any adaptations for non-commercial purposes.

ACS chemical biology

Articles

pubs.acs.org/acschemicalbiology

Imaging Complex Protein Metabolism in Live Organisms by Stimulated Raman Scattering Microscopy with Isotope Labeling

Lu Wei,[†] Yihui Shen,[†] Fang Xu,[†] Fanghao Hu,[†] Jamie K. Harrington,[‡] Kimara L. Targoff,[‡] and Wei Min*[,†,§]

[†]Department of Chemistry, [§]Kavli Institute for Brain Science, Columbia University, New York, New York 10027, United States

[‡]Department of Pediatrics, Columbia University, New York, New York 10032, United States

Supporting Information

ABSTRACT: Protein metabolism, consisting of both synthesis and degradation, is highly complex, playing an indispensable regulatory role throughout physiological and pathological processes. Over recent decades, extensive efforts, using approaches such as autoradiography, mass spectrometry, and fluorescence microscopy, have been devoted to the study of protein metabolism. However, noninvasive and global visualization of protein metabolism has proven to be highly challenging, especially in live systems. Recently, stimulated Raman scattering (SRS) microscopy coupled with metabolic labeling of deuterated amino acids (D-AAs) was demonstrated for use in imaging newly synthesized proteins in cultured cell lines. Herein, we significantly generalize this notion to develop a comprehensive labeling and imaging platform for live visualization of complex protein metabolism, including synthesis, degradation, and pulse−chase analysis of two temporally defined populations. First, the deuterium labeling efficiency was optimized, allowing time-lapse imaging of protein synthesis dynamics within individual live cells with high spatial−temporal resolution. Second, by tracking the methyl group (CH_3) distribution attributed to pre-existing proteins, this platform also enables us to map protein degradation inside live cells. Third, using two subsets of structurally and spectroscopically distinct D-AAs, we achieved two-color pulse−chase imaging, as demonstrated by observing aggregate formation of mutant hungtingtin proteins. Finally, going beyond simple cell lines, we demonstrated the imaging ability of protein synthesis in brain tissues, zebrafish, and mice *in vivo*. Hence, the presented labeling and imaging platform would be a valuable tool to study complex protein metabolism with high sensitivity, resolution, and biocompatibility for a broad spectrum of systems ranging from cells to model animals and possibly to humans.

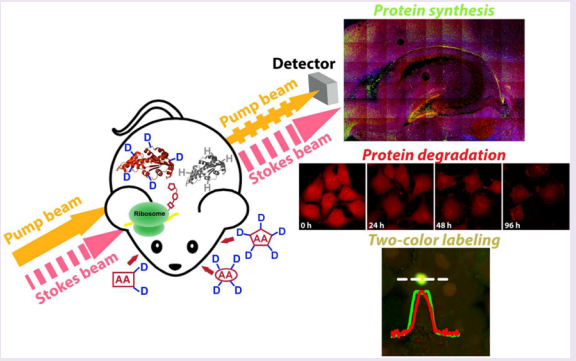

Proteins are dynamic entities in cells, acting coordinately through both synthesis and degradation to maintain cellular functions. Hence, the ability to image protein metabolism at a global level with subcellular resolution is extremely useful in revealing the metabolic status of a cell. Such a technique would enable functional identification of either subcellular compartments or cell locations within complex tissues during physiological and pathological processes. For example, long-term memory formation involves activity-dependent local protein synthesis in neurons,[1,2] whereas Huntington's disease often disrupts protein degradation pathways of the affected cells.[3,4] To some extent, it is not the identities of the proteins that are important, but the complex spatial distribution and temporal dynamics.

Current methods, including isotope-based analysis and bioorthogonal chemistry-based fluorescence detection, have been extensively applied to visualize complex metabolic dynamics at the proteome level. Traditional autoradiography using radioactive amino acids provides vigorous analysis for either protein synthesis or degradation.[5,6] However, samples must be fixed before exposure to films. Stable isotope labeling by amino acids in cell culture (SILAC) combined with mass spectrometry offers a quantitative approach for proteomics.[7,8] However, it lacks spatial information. Recently developed multi-isotope imaging mass spectrometry (MIMS) provides the imaging ability, but it is highly invasive and thereby not compatible with live systems.[9,10] A powerful fluorescence-based technique named bioorthogonal noncanonical amino acid tagging (BONCAT) was developed by metabolic incorporation of unnatural amino acids containing reactive groups, which are subsequently conjugated to fluorescent tags via click chemistry.[11−13] A related labeling strategy was demonstrated with an alkyne analogue of puromycin.[14] Unfortunately, these methods generally require nonphysiological fixation of cells.[15−17]

We have recently reported a live imaging technique to visualize nascent proteins by coupling stimulated Raman scattering (SRS) microscopy with metabolic labeling of deuterated amino acids (D-AAs) by a cell's native translational

Received: September 30, 2014
Accepted: January 5, 2015
Published: January 5, 2015

 © 2015 American Chemical Society

DOI: 10.1021/cb500787b
ACS Chem. Biol. 2015, 10, 901−908

machineries.[18] The newly synthesized proteins are specifically detected by SRS through the vibrational signature from carbon−deuterium bonds (C−D) in the cell-silent spectral region. This concept is particularly attractive for imaging *de novo* protein synthesis at the global level in live systems. On the labeling side, cells and animals can tolerate a large amount of deuterium on D-AAs, which introduces minimum perturbation to protein functions. In fact, experiments using deuterated water or deuterated drugs have already been carried out on humans.[19−21] On the imaging side, SRS microscopy is a sensitive and specific optical technique for imaging chemical bonds. When the energy difference between incident photons from two lasers (Pump beam and Stokes beam at 867.2 and 1064 nm, respectively) matches the 2133 cm^{-1} mode of C−D vibrations, the joint action of Pump and Stokes photons will efficiently excite a vibrational transition of C−D bonds. Whenever a molecule is transferred into the vibrational excited state, the Stokes pulse gains a photon, whereas the Pump pulse loses one, dictated by energy conservation (Figure 1a). By detecting the resulting stimulated Raman loss (or gain) of the Pump beam (or the Stokes beam) in one pixel and then raster scanning the laser spot across the sample, one can produce a 3D concentration map of the targeted C−D bonds in living cell and tissues (Figure 1b). Technically, SRS microscopy provides background-free chemical contrast with linear concentration dependence, subcellular resolution determined by the optical diffraction limit (*xy* resolution of ∼300 nm; *z* resolution or depth of field of ∼1000 nm), and intrinsic 3D sectioning that is suitable for tissue imaging, and the use of near-infrared wavelength and picosecond excitation pulses minimizes photon scattering inside turbid samples and potential phototoxicity.[22−25]

Despite the conceptual novelty, there are several notable shortcomings in the above proof-of-principle demonstration. First, only the synthesis aspect of protein metabolism was probed. Second, neither the D-AA labeling efficiency nor the SRS imaging instrument was optimized. Third, only cultured cell lines were demonstrated due to the limited sensitivity.[18]

In this article, we report a comprehensive labeling and imaging platform to probe complex protein metabolic dynamics by fully exploiting the notion of coupling SRS with metabolic labeling of D-AAs. Three major technical advances are being implemented together with a series of biological applications on complex tissues and model animals *in vivo* (Figure 1). First, we optimized the chemical composition of the deuterated culture medium to achieve a much higher deuterium labeling efficiency and improved imaging sensitivity and speed of our SRS instrumentation. These optimizations allow us to demonstrate time-lapse imaging of protein synthesis dynamics within single live cells. Second, we successfully imaged protein degradation in live HeLa cells by targeting the Raman peak of the methyl group (CH_3) for pre-existing protein pools and employing a recently developed linear combination algorithm on measured SRS images at 2940 and 2845 cm^{-1} channels. Third, inspired by the classic pulse−chase analysis of complex protein dynamics, two-color pulse−chase imaging was accomplished by rationally dividing D-AAs into two structurally different subsets that exhibit resolvable vibrational modes, as demonstrated by tracking aggregate formation of mutant huntingtin (mHtt) proteins. Finally, going beyond the cellular level to visualizing more complex tissues and animals *in vivo*, we imaged the spatial distribution of newly synthesized proteins inside live brain tissue slices and in both developmental embryonic zebrafish and mice (Figure 1). Taken together, these technical advances and biological applications demonstrate that SRS microscopy coupled with metabolic labeling of D-AAs is a comprehensive and generally applicable imaging platform to evaluate complex protein metabolism with high sensitivity, resolution, and biocompatibility in a broad spectrum of live cells, tissues, and animals.

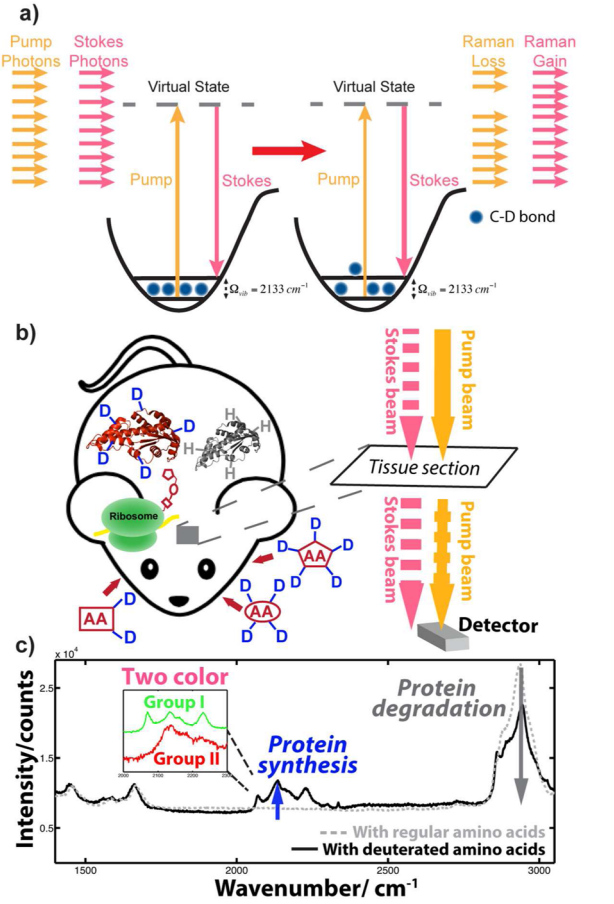

Figure 1. Imaging complex protein metabolism by stimulated Raman scattering (SRS) microscopy in live cells, tissues, and animals. (a) Energy diagram of the SRS process. (b) Cartoon for SRS imaging following metabolic labeling of deuterated amino acids (D-AAs) in live organisms (e.g., mice), which are first administered with D-AAs for a certain period of time and then imaged by SRS to probe protein metabolism. (c) Spontaneous Raman spectra from HeLa cells incubated with medium containing either regular amino acids (gray, dashed) or D-AAs (black, solid) illustrate three distinct ways to probe complex protein metabolism: imaging newly synthesized proteins by targeting 2133 cm^{-1} from carbon−deuterium bonds (C−D), imaging degradation of pre-existing proteins by targeting the pure methyl group (CH_3) distribution, and two-color pulse−chase protein imaging by labeling with two subgroups of D-AAs (i.e., groups I and II).

RESULTS AND DISCUSSION

Sensitivity Optimization and Time-Lapse Imaging of *de Novo* Proteome Synthesis Dynamics. The cell culture medium reported previously was prepared by supplying a uniformly deuterium-labeled whole set of amino acids to commercially available medium that is deficient in leucine, lysine, and arginine.[18] Due to the presence of other regular amino acids already in the commercial medium, the resulting partially deuterated medium has only about a 60% deuteration

DOI: 10.1021/cb500787b
ACS Chem. Biol. 2015, 10, 901−908

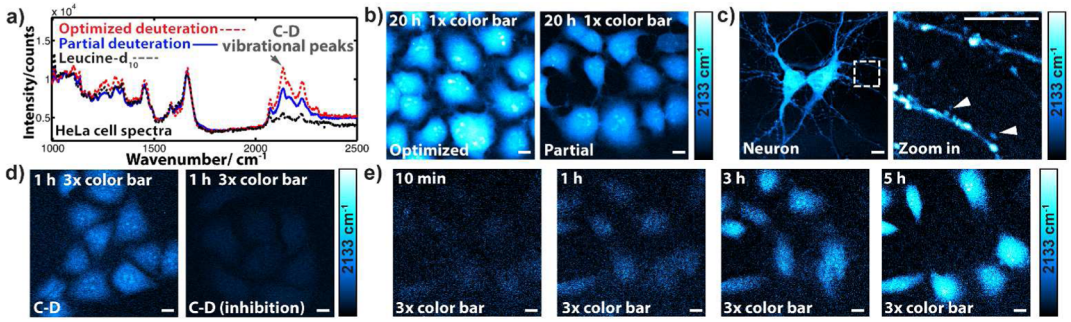

Figure 2. High-sensitivity SRS imaging of newly synthesized proteins in live cells after labeling and instrumentation optimization. (a) Spontaneous Raman spectrum of C−D peaks in HeLa cells incubated in optimized deuteration medium (red) displays a 50% increase when compared to that in the previously reported partial deuteration medium (blue) and is about 8 times higher than that using leucine-d_{10} (black) only. Each spectrum is averaged over 5−10 cells. (b) SRS images of newly synthesized proteins in live HeLa cells confirm a 50% average signal increase. (c) SRS images of newly synthesized proteins in live neurons in optimized deuteration medium for 20 h. The zoomed-in image highlights the fine dendritic structures (likely dendritic spines, arrow-headed). (d) SRS image of newly synthesized proteins in live HeLa cells with 1 h incubation of optimized deuteration medium. A control image with protein synthesis inhibition is deprived of most of the signal. (e) Time-lapse SRS images of protein synthesis dynamics in a same set of live HeLa cells with continuous incubation in optimized deuteration medium. Scale bar, 10 μm.

efficiency. In the present article, we custom-prepared new media that replace nearly all of the regular amino acids by the D-AA counterparts (details are given in the Supporting Information). As shown in the spontaneous Raman spectra (Figure 2a), the optimized medium (red spectrum) displays a 50% signal increase compared with that of the partially deuterated medium (blue spectrum). Indeed, SRS images targeting the C−D vibrational peak at 2133 cm^{-1} confirms a 50% average intensity boost in live HeLa cells (Figure 2b). The use of optimized D-AA medium now leads to an about 8 times higher signal than that when using a single leucine-d_{10} (Figure 2a, red vs black spectrum). In addition to improving the labeling strategy, nontrivial instrumentation optimizations were also carried out to further improve SRS detection sensitivity and acquisition speed, including increasing the laser output and microscope system's throughput for near-IR wavelengths, replacing the acousto-optic modulator (AOM) with an electro-optic modulator (EOM) for a 30% higher modulation depth, and employing a high-speed lock-in amplifier for faster image acquisition.

With much-improved sensitivity, protein synthesis can now be imaged with superb spatial and temporal resolution. Spatially, we visualized newly synthezied proteins from fine structures (likely dendritic spines, indicated by arrow heads) of live neurons (Figure 2c). Temporally, we could readily image newly synthesized proteins in live HeLa cells in less than a 1 h incubation with the optimized deuteration medium (Figure 2d). A control image of cells in the presence of protein synthesis inhibitors displays only vague and homogeneous cell outlines, which, presumably, come from the free D-AA pool (submillimolar concentration, much more dilute than the metabolically enriched pool in the protein-bound form).[18,26] Moreover, using a fast lock-in amplifier (details are given in Methods), our current imaging speed can be as fast as 3 s per frame (512 × 512 pixels), nearly 10 times faster than before, which enables time-lapse imaging in live cells with minimum phototoxicity to cell viabilities. Figure 2e presents time-lapse SRS imaging of the same set of live HeLa cells gradually synthesizing new proteins over time from a 10 min to 5 h incubation in optimized D-AA medium. The obvious observation of cell migration and division prove the viability of the cells, supporting the high biocompatibility of our technique. To our knowledge, this is the first time that long-term time-lapse imaging of proteome synthesis dynamics has been demonstrated on single live mamamian cells.

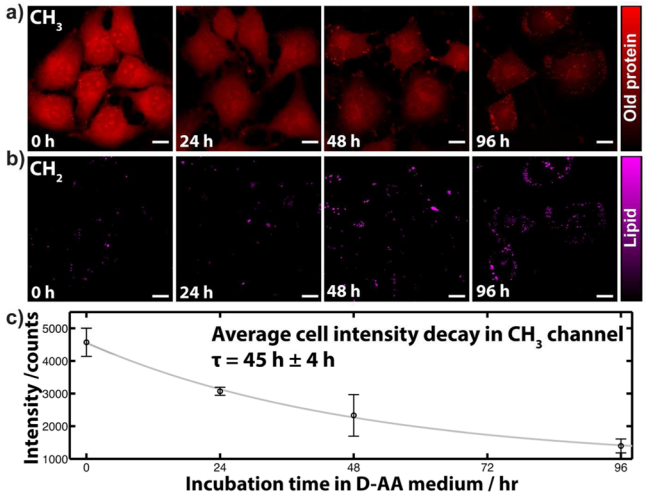

Figure 3. Time-dependent SRS imaging of protein degradation in live HeLa cells. (a) Adopting a linear combination algorithm between the 2940 and 2845 cm^{-1} channels, the obtained SRS images, exclusively from CH_3 vibration, display a gradual degradation of pre-existing proteins in live HeLa cells cultured in optimized deuteration medium for 0, 24, 48, and 96 h. (b) SRS images exclusively from CH_2 vibration display the total lipid distribution at the corresponding time point. (c) Single exponential decay fitting from averaged cellular image intensities of pre-existing proteins in panel a, yielding a protein degradation time constant of 45 ± 4 h. Error bars, standard deviation. Scale bar, 10 μm.

SRS Imaging of Protein Degradation in Live HeLa Cells. Besides imaging protein synthesis, our labeing and imaging platform offers the ability to probe protein degradation simultanously. Experimentally, we intend to probe the pre-existing protein pool by targeting CH_3, which shows a strong peak at 2940 cm^{-1}, as newly synthesized proteins will be mostly carrying C−D peaked around 2133 cm^{-1}. However, the 2940 cm^{-1} CH_3 protein channel is known to suffer from undesired crosstalk from the CH_2 lipid signal that peaks at 2845 cm^{-1}.[25] To obtain a clean protein component, we adopted two-color SRS imaging at both the 2940 and 2845 cm^{-1} channels followed by a linear combination algorithm that has been

DOI: 10.1021/cb500787b
ACS Chem. Biol. 2015, 10, 901−908

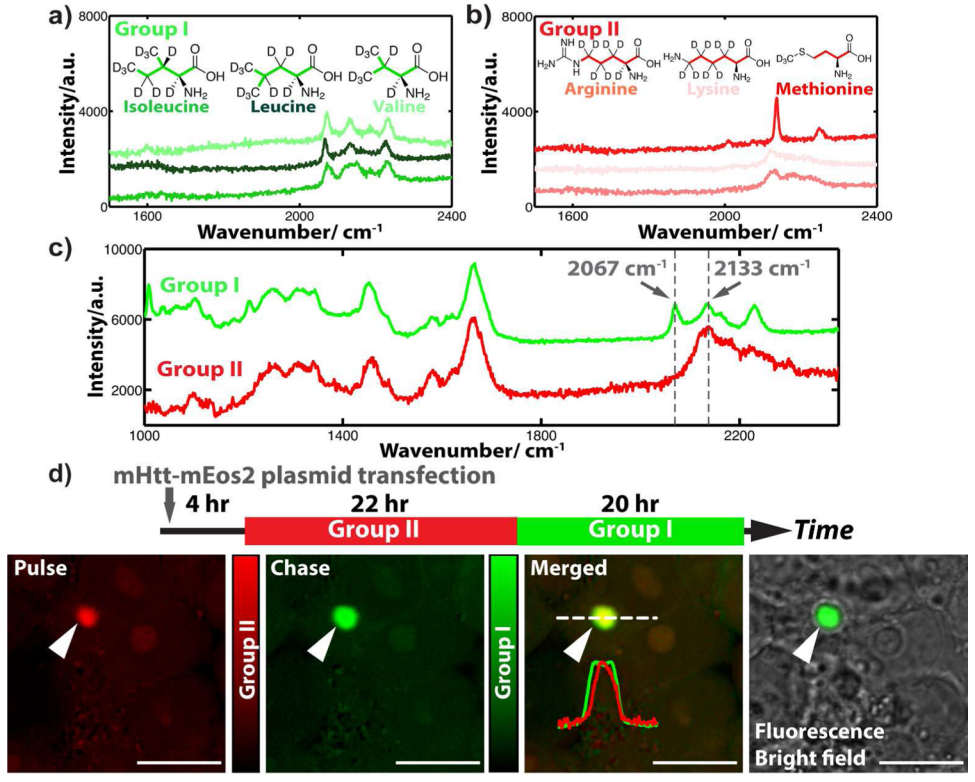

Figure 4. Two-color pulse−chase SRS imaging of two distinct sets of temporally defined proteins. (a) Structures and spontaneous Raman spectra of group I D-AAs (i.e., the branched-chain amino acids). (b) Structures and spontaneous Raman spectra of three examples of group II nonbranched D-AAs. (c) Spontaneous Raman spectra of HeLa cells cultured with group I D-AAs (green), showing multiple peaks, with the first being around 2067 cm^{-1}, and with group II D-AAs (red), showing a common peak around 2133 cm^{-1}. (d) Two-color pulse−chase imaging by sequential labeling of group II and group I D-AAs in time with simultaneous expression of mutant huntingtin (mHtt94Q-mEos2) proteins. The cartoon displays the experimental timeline of plasmid transfection and D-AA medium exchanges. The fluorescence image (overlaid with the bright-field image) indicates the formation of a large aggregate (arrow head) of mHtt94Q-mEos2. The retrieved signals from a linear combination of the original images from the 2067 and 2133 cm^{-1} channels display a large aggregation of mHtt proteins labeled solely by group II D-AAs during the first 22 h (red, pulse) and mHtt proteins labeled only by group I D-AAs during the following 20 h (green, chase). The merged image, as well as the intensity profile, from the pulsed (red) and chased (green) images confirms this with its yellow core and green shell. Scale bar, 10 μm.

effectively applied in cells, tissues, and animals.[27−29] The subsequently obtained images show the pure distribution of old protein pools (exclusively from CH_3) and the distribution of lipids (exclusively from CH_2), respectively. Hence, protein degradation could be tracked by imaging the old protein distributions over time when cells are growing in D-AA medium.

Figure 3a shows time-dependent SRS images of old protein distributions (CH_3) in live HeLa cells when incubated with D-AAs from 0 to 96 h. Clearly, the old protein pool is degrading, as shown by the decay of its average intensity. In contrast, the total lipid images display no obvious intensity change (Figure 3b). In addition, the spatial patterns of old proteins (Figure 3a) reveal a faster decay in the nucleoli than that in the cytoplasm. This observation is consistent with the fact that neucleoli have active protein turnover[30] and also with our previous report that C−D labeled newly synthesized proteins are more prominent in nucleoli.[18] Single exponential decay fitting of the average intensities in Figure 3a yields a decay time constant of 45 ± 4 h (Figure 3c), corresponding to a proteome half-life of 31 ± 3 h, which is very close to that reported by mass spectrometry (35 h).[31] Therefore, our imaging platform is capable of observing both protein synthesis and degradation by imaging the C−D channel and CH_3 channel, respectively, thus capturing proteomic metabolism dynamics in full-scope.

Two-Color Pulse−Chase SRS Imaging of Two Sets of Temporally Defined Proteins. Inspried by the popular pulse−chase analysis employed in classic autoradiography techniques and recent two-color BONCAT imaging,[32] we aimed to exploit another dimension of probing dynamic protein metabolism with two-color pulse−chase imaging of proteins labeled at different times. To do so, we need to rationally divide total D-AAs into two subsets with distinct Raman spectra. We reasoned that Raman peaks of C−D stretching are closely related to their chemical environments; thus, the structural difference between D-AAs should lead to diverse Raman peak positions and shapes. We then examined the spontaneous Raman spectra of each D-AA sequentially and subsequently identified two subgroups. Group I contains three amino acids, leuine-d_{10}, isoleucine-d_{10}, and valine-d_8, structurally known as branched-chain amino acids (Figure 4a). All members of group I exhibit multiple distinct Raman peaks, with the first one being around 2067 cm^{-1}. The rest of the D-AAs without branched chains are then categorized into group II, all of which show a prominent Raman peak around 2133 cm^{-1} (three examples are shown in Figure 4b). To test this inside cells, Raman spectra of HeLa cells cultured in either group I D-AA medium only (green) or group II D-AA medium only (red) are shown in Figure 4c. On the basis of the spectra, we chose to acquire two-color narrow-band SRS images at 2067 and 2133 cm^{-1}. By

DOI: 10.1021/cb500787b
ACS Chem. Biol. 2015, 10, 901−908

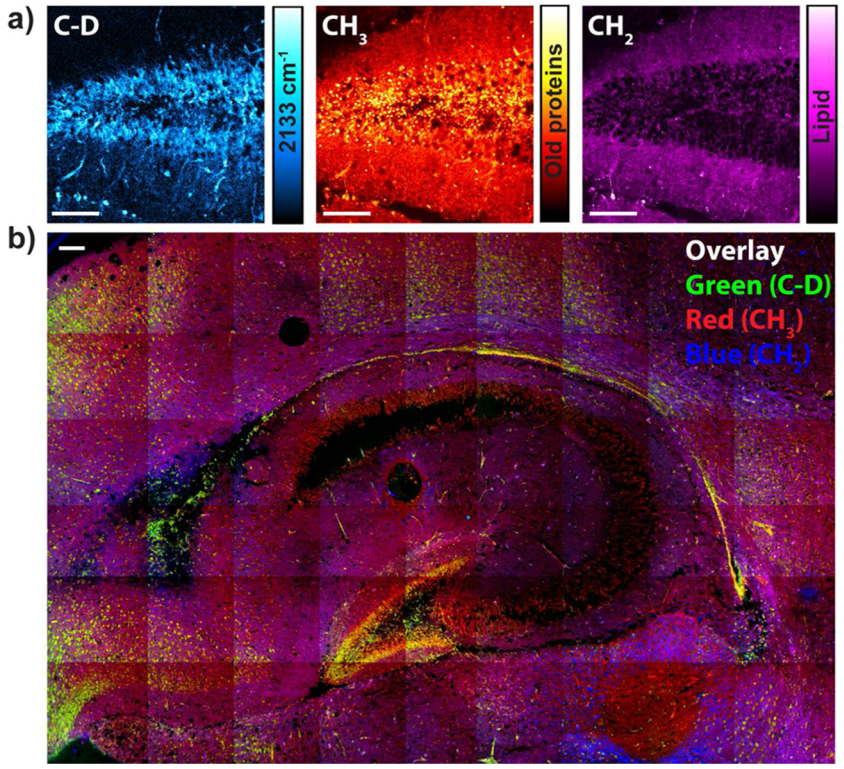

Figure 5. SRS imaging of live mouse brain tissues identifying the locations of active protein synthesis. (a) SRS images of the dentate gyrus of a live organotypic brain slice (400 μm thick, from a P10 mouse) after culturing in D-AA medium for 30 h. The 2133 cm^{-1} (C−D) image presents the distribution of newly synthesized proteins. The CH_3 and CH_2 images show the old protein pool and total lipid, respectively. (b) A 4 × 3 mm^2 large-field view overlay image of new proteins (C−D, green), old proteins (CH_3, red), and total lipids (CH_2, blue) for a brain slice (400 μm thick, from a P12 mouse) cultured in D-AA medium for 30 h. Scale bar, 100 μm.

constructing and utilizing a linear combination algorithm (Supplementary Figure 1), similar to the one used for CH_3 and CH_2 above, pure signals of proteins labeled by group I D-AAs and by group II D-AAs can be successfully separated and quantitatively visualized. Note that hyperspectral imaging approaches using broadband femtosecond lasers might also work here.[33−35]

We now chose the mutant huntingtin (mHtt) protein in Huntington's disease as our model system for the pulse−chase imaging demonstration. It is believed that Huntington's disease is caused by a mutation from a normal huntingtin gene to a mHtt gene expressing aggregation-prone mHtt proteins with polyglutamine (polyQ) expansion.[3] For easy visualization by fluorescence, we tagged mHtt (with 94Q) with a fluorescent protein marker, mEos2. As illustrated by the cartoon in Figure 4d, HeLa cells were first transfected with mHtt94Q-mEos2 plasmid in regular medium for 4 h, which was then replaced with group II D-AA medium for 22 h before changing to group I D-AA medium for another 20 h. SRS images are acquired in the 2067 and 2133 cm^{-1} channels, respectively, and subsequently processed with linear combination.

A fluorescence image overlaid with a bright-field image demonstrates the formation of a large aggregate triggered by aggregation-prone polyQ expansion in mHtt94Q-mEos2 (Figure 4d, fluorescence). Interestingly, proteins labeled with group II D-AAs during the initial pulse period concentrate mainly within the core of the aggregate (Figure 4d, red), whereas proteins labeled with group I D-AAs during the subsequent chase period occupy the entire volume of the aggregate (Figure 4d, green). The merged image between group I and group II images, as well as the intensity profiles across the aggregate, further confirm the observation of a yellow core inside and a green shell outside (Figure 4d, merged). This two-color pulse−chase result suggests that the core is aggregated earlier in time and that the later produced mHtt proteins are then recruited to and percolate through the aggregate to increases its overall size, in agreement with recently reported results by fluorescence.[36] The demonstration here thus illustrates that our imaging platform using the two subgroups of D-AAs is readily applicable for performing pulse−chase imaging to probe the complex and dynamic aspects of proteome metabolism.

SRS Imaging of Newly Synthesized Proteins in Live Mouse Brain Tissues. Going above the cellular level, we now apply our imaging platform to a more complex level, organotypical brain tissues. In our study, we focus on the hippocampus because it is the key region in brains that involves extensive protein synthesis.[5,37] As expected, active protein synthesis is found in the hippocampal region, particularly in the dentate gyrus, which is known for its significant role in both long-term memory formation and adult neurogenesis.[37] An SRS image at 2133 cm^{-1} (Figure 5a, C−D) of a live mouse organotypic brain slice cultured in D-AA medium for 30 h reveals active protein synthesis from both the soma and neurites of individual neurons in the dentate gyrus. In addition, the old protein (CH_3) and total lipid (CH_2) images are presented silmultaneously for multichannel analysis (Figure 5a).

In order to investigate spatial pattern of protein synthesis on a larger scale, we imaged the entire brain slice by acquiring

DOI: 10.1021/cb500787b
ACS Chem. Biol. 2015, 10, 901−908

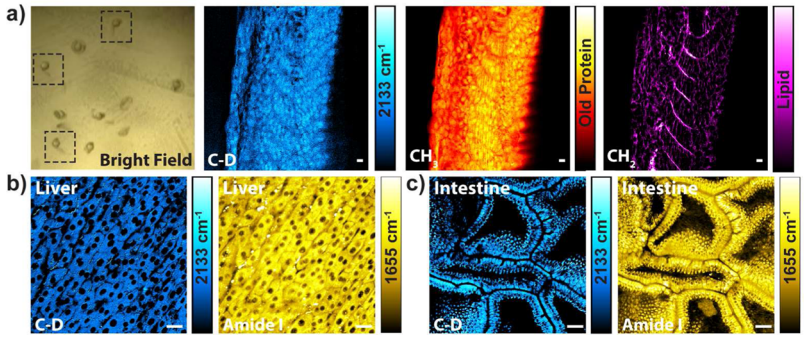

Figure 6. SRS imaging for newly synthesized proteins *in vivo*. (a) SRS images of a 24 hpf (hpf, hours post fertilization) zebrafish. Wild-type zebrafish embryos were injected at the 1-cell stage with 1 nL of D-AA solution and allowed to develop normally for another 24 h before imaging. The bright-field image shows the gross morphology of embryonic zebrafish at 24 hpf (dashed boxes). The 2133 cm^{-1} (C−D) image presents the distribution of newly synthesized proteins (Supplemental Figure 2a) in the somites of an embryonic zebrafish tail. The CH_3 image shows the old protein pool, whereas the CH_2 image depicts total lipid in the same fish. (b, c) SRS images of live mouse liver (b) and intestine (c) tissues harvested from mice after being administered with D-AA-containing drinking water for 12 days. The 2133 cm^{-1} (C−D) channel shows newly synthesized proteins (Supplemental Figure 2b,c) that resemble the distribution of total protein as that shown in the 1655 cm^{-1} image (amide I). Scale bar, 10 μm.

large-area image mosaics. A 4 × 3 mm^2 image (Figure 5b) of another organotypic slice displays an overlaid pattern from new proteins (2133 cm^{-1}, green), old proteins (CH_3, red), and lipids (CH_2, blue). Intriguing spatial variation is observed: while the distribution of old proteins is relatively homogeneous across the field of view, newly synthesized proteins are either concentrated in the dentate gyrus or scattered within individual neurons throughout the cortex, suggesting high activity in these two regions. Thus, we have demonstrated the ability to directly image protein synthesis dynamics on living brain tissues with subcellular resolution and multichannel analysis, which was difficult to achieve with other existing methods.[38] The intricate relationship between protein synthesis and neuronal plasticity[39] is currently under investigation on this platform.

SRS Imaging of Newly Synthesized Proteins *in Vivo*. One prominent advantage of our labeling strategy is its nontoxicity and minimal invasiveness to animals. We thus move up to the physiological level to image protein metabolism in embryonic zebrafish and mice. Zebrafish are popular model organisms due to their well-understood genetics and transparent embryos, amenable to optical imaging.[40] We injected 1 nL of D-AA solution into zebrafish embryos at the 1-cell stage (150 ng of D-AAs per embryo) and then allowed them to develop normally for 24 h (Figure 6a, bright field) before imaging the whole animal. We found a high signal of newly synthesized proteins (Figure 6a, 2133 cm^{-1}) in the somites at the embryonic zebrafish tail, consistent with the earlier BONCAT result.[41] The spatial pattern of this signal appears to be similar to that of the old protein distribution (Figure 6a, CH_3), but it is almost complementary to the lipid distribution (Figure 6a, CH_2).

Finally, we demonstrate this approach on mammals (mice). We administered drinking water containing D-AAs to 3 week old mice for 12 days and then harvested their liver and intestine tissues for subsequent imaging. No toxicity was observed for the fed mice. SRS images from both live liver tissues (Figure 6b) and live intestine tissues (Figure 6c) illustrate the distributions of newly synthesized proteins (2133 cm^{-1}, C−D) during the feeding period, which resembled the total protein distribution (1655 cm^{-1}, amide I). On a faster incoporation time scale, live liver and intestine tissues obtained after intraperitoneal injection of D-AAs into mice for 36 h reveal spatial patterns (Supplemental Figure 3) similar to those of the feeding results above as well as the click chemistry-based fluorescence staining.[14] All of these results are in support of our imaging platform being a highly suitable technique for *in vivo* interrogation.

Conclusions. The ability to probe complex proteome metabolism with high sensitivity, resolution, and biocompatibility will help us to gain deep insight into protein metabolic regulation in biological systems under healthy and diseased conditions. We have thus presented such a platform by coupling SRS imaging with metabolic labeling of D-AAs. First, we achieved optimized labeling and imaging of *de novo* protein sythesis in live cancer cells and neurons as well as time-lapse dynamic imaging with much improved spatial−temporal resolution than that in our previous demonstration. Then, we developed new experimental approaches to image protein degradation and temporally distinct protein populations in live cells. Thus, we have generalized the utility of this approach from the previous imaging of protein synthesis only to including protein degradation and complex two-color pulse−chase dynamics. Finally, we extended the use of this approach from the cellular level to the more complex tissue level and all of the way to *in vivo* animal visualization.

Technically, compared to existing methods for probing proteomes such as BONCAT, SILAC, and MIMS, our technique is mostly superior in its biocompatibility, thanks to the unique coupling of stable isotope labeling with SRS imaging, which also brings significant advantages in terms of specific utilities of the platform. The bioorthognality of C−D together with the background-free nature of SRS microscopy render protein synthesis detection to be highly sensitive and selective; for protein degradation, the linear concentration dependence and the Raman spectral fidelity of SRS allow quantitative retrieval of the pure CH_2 and CH_3 signals; for two-color imaging, the narrow-band SRS excitation using pico-second pulses permits the rich spectral diversity of D-AAs to be exploited for coding distinct protein populations. All of these technical advantages are difficult to achieve by coherent anti-stokes Raman scattering (CARS), which is known for its nonresonant background, nonlinear dependence on analyte concentrations, and severe spectral distortion.[25]

Biologically, the presented platform will pave the way for interogating a broad range of complex systems, such as memory-related protein systhesis in hippocampal brain tissues,

DOI: 10.1021/cb500787b
ACS Chem. Biol. 2015, 10, 901−908

protein aggregation and degradation in neurodegenerative diseases, and protein metabolism in animal disease models. Furthermore, considering that stable isotope labeling and SRS imaging are both compatible with live humans,[42] we envision that the prospects are bright for applying this platform to performing diagnostic and theraputic imaging in humans.

METHODS

Stimulated Raman Scattering Microscopy. Spatially and temporally overlapped pulsed Pump (tunable from 720 to 990 nm, 5−6 ps, 80 MHz repetition rate) and Stokes (1064 nm, 6 ps, 80 MHz repetition rate, modulated at 8 MHz) beams, which are provided by a custom-modified picoEMERALD system from Applied Physics & Electronics, Inc., are coupled into an inverted laser-scanning microscope (FV1200 MPE, Olympus) optimized for near-IR throughput. A 60× water objective (UPlanAPO/IR, 1.2 N.A., Olympus) is used for all cell imaging, and a 25× water objective (XLPlan N, 1.05 N.A., MP, Olympus) with both a high near-IR transmission and a large field of view is used for brain tissue and *in vivo* imaging. After passing through the sample, the forward-going Pump and Stokes beams are collected in transmission by a high N.A. oil condenser. A high O.D. bandpass filter (890/220, Chroma) is used to block the Stokes beam completely and to transmit the Pump beam only onto a large area Si photodiode for the detection of the stimulated Raman loss signal. The output current from the photodiode is terminated, filtered, and demodulated by a lock-in amplifier at 8 MHz to ensure shot-noise-limited detection sensitivity. (Details are given in the Supporting Information.)

Metabolic Incorporation of Deuterated Amino Acids. For HeLa cells, cells were seeded on a coverslip in a Petri dish with 2 mL of regular medium for 20 h, which was then replaced with D-AA medium (or group I and group II D-AA media) for the designated amount of time. The coverslip was taken out to make an imaging chamber filled with PBS for SRS imaging. For hippocampal neurons, the dissociated neurons from newborn mice were seeded for 10 days in regular Neurobasal A medium, which was then replaced with the corresponding D-AA medium for the designated amount of time before imaging. For organotypic brain slices, 400 μm thick, P10 mouse brain slices were cultured on Millicell-CM inserts (PICM03050, Millipore) in 1 mL of CD-MEM culture medium for 2 h, which was then changed to 1 mL of CD-neurobasal A culture medium for another 28 h before imaging. For a detailed recipe of D-AA media and the *in vivo* labeling procedure in zebrafish and mice, see the Supporting Information. The experimental protocols for *in vivo* mice experiments (AC-AAAG2702) and zebrafish experiments (AC-AAAD6300) were approved by the Institutional Animal Care and Use Committee at Columbia University.

Spontaneous Raman spectroscopy. The spontaneous Raman spectra were acquired using a laser Raman spectrometer (inVia Raman microscope, Ranishaw) at room temperature. A 27 mW (after objective), 532 nm diode laser was used to excite the sample through a 50×, N.A. 0.75 objective (NPLAN EPI, Leica). The total data acquisition was performed during 60 s using WiRE software. All of the spontaneous Raman spectra subtracted the PBS solution as background.

Image Progressing. Images were acquired with FluoView scanning software and assigned color or overlaid by ImageJ. Linear combination was processed with MATLAB. Graphs were assembled with Adobe Illustrator.

ASSOCIATED CONTENT

Supporting Information

Additional materials and methods. Figure S1: SRS images at 2067 and 2133 cm^{-1} channels of proteins labeled with group I D-AA only and group II D-AA only. Figure S2: Raw C-D on-resonance (2133 cm^{-1}) and off-resonance (2000 cm^{-1}) SRS images of newly synthesized proteins *in vivo*. Figure S3: SRS imaging for newly synthesized proteins *in vivo* with intraperitoneal injection of mice with D-AA solutions. This material is available free of charge via the Internet at http://pubs.acs.org.

AUTHOR INFORMATION

Corresponding Author

*E-mail: wm2256@columbia.edu.

Author Contributions

L.W., Y.S., F.X., F.H., J.K.H., and K.L.T. performed experiments and analyzed data. L.W., Y.S., and W.M. designed the experiments. L.W. and W.M. conceived the concept and wrote the article.

Notes

The authors declare the following competing financial interest(s): Columbia University has filed a patent application based on this work.

ACKNOWLEDGMENTS

We thank J. Jackson and C. Dupre for assistance with the brain slices and J. C. Tapia, M. C. Wang, Z. Chen, D. Peterka, and R. Yuste for helpful discussions. We are grateful to Y. Shin for technical assistance with the *in vivo* mice experiments. W.M. acknowledges support from Columbia University, an National Institutes of Health Director's New Innovator Award, the U.S. Army Research Office (W911NF-12-1-0594), the Brain Research Foundation, and an Alfred P. Sloan Research Fellowship.

REFERENCES

(1) Mayford, M., Siegelbaum, S.-A., and Kandel, E.-R. (2012) Synapses and memory storage. *Cold Spring Harbor Perspect. Biol. 4*, a005751.

(2) Sutton, M.-A., and Schuman, E.-M. (2006) Dendritic protein synthesis, synaptic plasticity, and memory. *Cell 127*, 49−58.

(3) Walker, F.-O. (2007) Huntington's disease. *Lancet. 369*, 218−228.

(4) Bennett, E.-J., Shaler, T.-A., Woodman, B., Ryu, K.-Y., Zaitseva, T.-S., Becker, C.-H., Bates, G.-P., Schulman, H., and Kopito, R. R. (2007) Global changes to the ubiquitin system in Huntington's disease. *Nature 448*, 704−708.

(5) Lipton, P., and Raley-Susman, K.-M. (1999) Autoradiographic measurements of protein synthesis in hippocampal slices from rats and guinea pigs. *Methods 18*, 127−143.

(6) Bachmair, A., Finley, D., and Varshavsky, A. (1986) *In vivo* half-life of a protein is a function of its amino-terminal residue. *Science 234*, 179−186.

(7) Ong, S.-E., Blagoev, B., Kratchmarova, I., Kristensen, D.-B., Steen, H., Pandey, A., and Mann, M. (2002) Stable isotope labeling by amino acids in cell culture, SILAC, as a simple and accurate approach to expression proteomics. *Mol. Cell. Proteomics 1*, 376−386.

(8) Mann, M. (2006) Functional and quantitative proteomics using SILAC. *Nat. Rev. Mol. Cell Biol. 7*, 952−958.

(9) Lechene, C., Hillion, F., McMahon, G., Benson, D., Kleinfeld, A.-M., Kampf, J.-P., Distel, D., Luyten, Y., Bonventre, J., Hentschel, D., Park, K.-M., Ito, S., Schwartz, M., Benichou, G., and Slodzian, G. (2006) High-resolution quantitative imaging of mammalian and bacterial cells using stable isotope mass spectrometry. *J. Biol. 5*, 20.

(10) Zhang, D.-S., Piazza, V., Perrin, B.-J., Rzadzinska, A.-K., Poczatek, J.-C., Wang, M., Prosser, H.-M., Ervasti, J.-M., Corey, D.-P., and Lechene, C.-P. (2012) Multi-isotope imaging mass spectrometry reveals slow protein turnover in hair-cell stereocilia. *Nature 481*, 520−524.

(11) Beatty, K.-E., Liu, J.-C., Xie, F., Dieterich, D.-C., Schuman, E.-M., Wang, Q., and Tirrell, D.-A. (2006) Fluorescence visualization of newly synthesized proteins in mammalian cells. *Angew. Chem., Int. Ed. 45*, 7364−7367.

DOI: 10.1021/cb500787b
ACS Chem. Biol. 2015, 10, 901−908

(12) Ngo, J.-T., and Tirrell, D.-A. (2011) Noncanonical amino acids in the interrogation of cellular protein synthesis. *Acc. Chem. Res. 44*, 677−685.
(13) Yuet, K.-P., and Tirrell, D.-A. (2014) Chemical tools for temporally and spatially resolved mass spectrometry-based proteomics. *Ann. Biomed. Eng. 42*, 299−311.
(14) Liu, J., Xu, Y., Stoleru, D., and Salic, A. (2012) Imaging protein synthesis in cells and tissues with an alkyne analog of puromycin. *Proc. Natl. Acad. Sci. U.S.A. 109*, 413−418.
(15) Prescher, J.-A., and Bertozzi, C.-R. (2005) Chemistry in living systems. *Nat. Chem. Biol. 1*, 13−21.
(16) Bertozzi, C.-R. (2011) A decade of bioorthogonal chemistry. *Acc. Chem. Res. 44*, 651−653.
(17) Grammel, M., and Hang, H.-C. (2013) Chemical reporters for biological discovery. *Nat. Chem. Biol. 9*, 475−484.
(18) Wei, L., Yu, Y., Shen, Y., Wang, M.-C., and Min, W. (2013) Vibrational imaging of newly synthesized proteins in live cells by stimulated Raman scattering microscopy. *Proc. Natl. Acad. Sci. U.S.A. 110*, 11226−11231.
(19) Moore, F.-D. (1946) Determination of total body water and solids with isotopes. *Science 104*, 157−160.
(20) Pinkus, J.-L., Charles, D., and Chattoraj, S.-C. (1971) Deuterium-labeled steroids for study in humans: I. estrogen production rates in normal pregnancy. *J. Biol. Chem. 246*, 633−636.
(21) Tang, G., Qin, J., and Dolnikowski, G.-G. (1998) Deuterium enrichment of retinol in humans determined by gas chromatography electron capture negative chemical ionization mass spectrometry. *J. Nutr. Biochem. 9*, 408−414.
(22) Freudiger, C.-W., Min, W., Saar, B.-G., Lu, S., Holtom, G.-R., He, C., Tsai, J.-C., Kang, J.-X., and Xie, X.-S. (2008) Label-free biomedical imaging with high sensitivity by stimulated Raman scattering microscopy. *Science 322*, 1857−1861.
(23) Min, W. (2011) Label-free optical imaging of nonfluorescent molecules by stimulated radiation. *Curr. Opin. Chem. Biol. 15*, 831−837.
(24) Min, W., Freudiger, C.-W., Lu, S., and Xie, X.-S. (2011) Coherent nonlinear optical imaging: beyond fluorescence microscopy. *Annu. Rev. Phys. Chem. 62*, 507−530.
(25) (2012) *Coherent Raman Scattering Microscopy* (Cheng, J.-X., and Xie, X.-S., Eds.) CRC Press, Boca Raton, FL.
(26) Piez, K.-A., and Eagle, H. (1958) The free amino acid pool of cultured human cells. *J. Biol. Chem. 231*, 533−545.
(27) Lu, F.-K., Ji, M., Fu, D., Ni, X., Freudiger, C.-W., Holtom, G., and Xie, X.-S. (2012) Multicolor stimulated Raman scattering (SRS) microscopy. *Mol. Phys. 110*, 1927−1932.
(28) Yu, Z., Chen, T., Zhang, X., Fu, D., Liao, X., Shen, J., Liu, X., Zhang, B., Xie, X.-S., Su, X.-D., Chen, J., and Huang, Y. (2012) Label-free chemical imaging *in vivo*: three-dimensional non-invasive microscopic observation of amphioxus notochord through stimulated Raman scattering (SRS). *Chem. Sci. 3*, 2646−2654.
(29) Ji, M., Orringer, D.-A., Freudiger, C.-W., Ramkissoon, S., Liu, X., Lau, D., Golby, A.-J., Norton, I., Hayashi, M., Agar, N.-Y., Young, G.-S., Spino, C., Santagata, S., Camelo-Piragua, S., Ligon, K.-L., Sagher, O., and Xie, X.-S. (2013) Rapid, label-free detection of brain tumors with stimulated Raman scattering microscopy. *Sci. Transl. Med. 5*, 201ra119.
(30) Andersen, J.-S., Lam, Y.-W., Leung, A.-K., Ong, S.-E., Lyon, C.-E., Lamond, A.-I., and Mann, M. (2005) Nucleolar proteome dynamics. *Nature 433*, 77−83.
(31) Cambridge, S.-B., Gnad, F., Nguyen, C., Bermejo, J.-L., Krüger, M., and Mann, M. (2011) Systems-wide proteomic analysis in mammalian cells reveals conserved, functional protein turnover. *J. Proteome Res. 10*, 5275−5284.
(32) Beatty, K.-E., and Tirrell, D.-A. (2008) Two-color labeling of temporally defined protein populations in mammalian cells. *Bioorg. Med. Chem. Lett. 18*, 5995−5999.
(33) Zhang, D., Wang, P., Slipchenko, M.-N., Ben-Amotz, D., Weiner, A.-M., and Cheng, J.-X. (2013) Quantitative vibrational imaging by hyperspectral stimulated Raman scattering microscopy and multivariate curve resolution analysis. *Anal. Chem. 85*, 98−106.
(34) Zhang, D., Slipchenko, M.-N., and Cheng, J.-X. (2011) Highly sensitive vibrational imaging by femtosecond pulse stimulated Raman loss. *J. Phys. Chem. Lett. 2*, 1248−1253.
(35) Fu, D., Holtom, G., Freudiger, C.-W., Zhang, X., and Xie, X.-S. (2013) Hyperspectral imaging with stimulated Raman scattering by chirped femtosecond lasers. *J. Phys. Chem. B 117*, 4634−4640.
(36) Schipper-Krom, S., Juenemann, K., Jansen, A.-H., Wiemhoefer, A., van den Nieuwendijk, R., Smith, D.-L., Hink, M.-A., Bates, G.-P., Overkleeft, H., Ovaa, H., and Reits, E. (2014) Dynamic recruitment of active proteasomes into polyglutamine initiated inclusion bodies. *FEBS Lett. 588*, 151−159.
(37) Deng, W., Aimone, J.-B., and Gage, F.-H. (2010) New neurons and new memories: how does adult hippocampal neurogenesis affect learning and memory? *Nat. Rev. Neurosci. 11*, 339−350.
(38) Dieterich, D.-C., Hodas, J.-J., Gouzer, G., Shadrin, I.-Y., Ngo, J.-T., Triller, A., Tirrell, D.-A., and Schuman, E.-M. (2010) *In situ* visualization and dynamics of newly synthesized proteins in rat hippocampal neurons. *Nat. Neurosci. 13*, 897−905.
(39) Hinz, F.-I., Dieterich, D.-C., and Schuman, E.-M. (2013) Teaching old NCATs new tricks: using non-canonical amino acid tagging to study neuronal plasticity. *Curr. Opin. Chem. Biol. 17*, 738−746.
(40) Kari, G., Rodeck, U., and Dicker, A.-P. (2007) Zebrafish: an emerging model system for human disease and drug discovery. *Clin. Pharmacol. Ther. 82*, 70−80.
(41) Hinz, F.-I., Dieterich, D.-C., Tirrell, D.-A., and Schuman, E.-M. (2012) Non-canonical amino acid labeling *in vivo* to visualize and affinity purify newly synthesized proteins in larval zebrafish. *ACS Chem. Neurosci. 3*, 40−49.
(42) Saar, B.-G., Freudiger, C.-W., Reichman, J., Stanley, C.-M., Holtom, G.-R., and Xie, X.-S. (2010) Video-rate molecular imaging in vivo with stimulated Raman scattering. *Science 330*, 1368−1370.

DOI: 10.1021/cb500787b
ACS Chem. Biol. 2015, 10, 901−908